

Stable lifetime of compact, evenly-spaced planetary systems with non-equal masses

David R. Rice,¹^{*} and Jason H. Steffen¹

¹*Department of Physics & Astronomy, University of Nevada, Las Vegas, 4505 S. Maryland Pkwy., Las Vegas, NV 89154, USA*

Accepted XXX. Received YYY; in original form ZZZ

ABSTRACT

Compact planetary systems with more than two planets can undergo orbital crossings from planet-planet perturbations. The time which the system remains stable without orbital crossings has an exponential dependence on the initial orbital separations in units of mutual Hill radii. However when a multiplanet system has period ratios near mean-motion resonances, its stability time differs from the time determined by planet separation. This difference can be up to an order of magnitude when systems are set up with chains of equal period ratios. We use numerical simulations to describe the stability time relationship in systems with equal separations but non-equal masses which breaks the chains of equal period ratios. We find a deviation of 30 per cent in the masses of the planets creates a large enough deviation in the period ratios where the average stability time of a given spacing can be predicted by the stability time relationship. However, the distribution of stability time at a given spacing is much wider than in equal-mass systems. We find the stability time distribution is heteroscedastic with spacing—the deviation in stability time for a given spacing increases with said spacing.

Key words: planets and satellites: dynamical evolution and stability – methods: numerical

1 INTRODUCTION

The dynamical spacing of a system influences how a post-gas disc system evolves through planet-planet interactions (Fang & Margot 2013; Volk & Gladman 2015). In a closely-packed system, the planets' eccentricities grow from planet-planet perturbations until an orbital crossing occurs. A crossing can be marked by a close encounter of two planets after which the system experiences chaotic orbital evolution until a collision or ejection occurs. The lifetime of the stable system before the instability occurs is dependent on the initial spacing between the planets.

Within a critical spacing, a system's orbits are always chaotic because of overlapping two-body resonances (Deck et al. 2013). These resonances are important to observed systems as several multiplanet systems have confirmed resonance chains where multiple bodies are in two- and three-body resonances (Mills et al. 2016; MacDonald et al. 2016; Luger et al. 2017; MacDonald et al. 2022). However, the typical planetary system found by Kepler is not in resonance (Fabrycky et al. 2014; Steffen & Hwang 2015). A planetary system's dynamical spacing and closeness to resonance can be used to assess its long term stability.

Obertas et al. (2017) studies the relationship between stability time and dynamical spacing measured in mutual Hill radii (Eq. 1) with over 10,000 simulations. They use systems of five Earth-mass planets on co-planar and circular orbits with a solar-mass star. As

described in previous work starting with Chambers et al. (1996), they find a strong, exponential relationship where the stability time increases by approximately an order of magnitude with every integer increase in mutual Hill radii spacing between planets.

The use of equal-mass bodies with equal Hill separations implies that the bodies are in equal period ratios. This artificial setup places the planets in chains of resonance that cause perturbations at regular intervals between the bodies. In Obertas et al. (2017), systems with adjacent or next-adjacent planets near first or second-order mean-motion resonances (MMR) have stability times that deviate from the time predicted by the spacing. Also reported in Chambers et al. (1996); Marzari & Weidenschilling (2002); Pu & Wu (2015), the chains of MMR in these multi-planet systems cause separation-dependent modulations superimposed on the stability time relationship that have amplitudes as large as an order of magnitude.

Chambers et al. (1996) integrates 120 systems of 20 planets with equal spacing and masses that vary by a factor of five. Their results suggest that variable masses “smooth out” the stability time relationship erasing the MMR modulations. Here, we investigate with much higher resolution the use of variable masses in more-restricted 4 planet systems with equal Hill spacing. We detail the amount of mass variation and its corresponding period ratio variation needed to smooth out the stability time relationship. We detail how inhomogeneities in a system's masses widen the distribution of stability time resulting in a heteroscedastic stability time relationship with spacing.

* E-mail: david.rice@unlv.edu

Our paper is laid out as follows. In Section 2 and Section 3, we describe the relevant parameters to our study and the setup of our planetary systems. We reproduce the resonant deviations in stability time for systems with equal-mass and equal-spacing in Section 4. We then model systems with equal-spacing but use variable mass planets in Section 5. Finally, in Section 6 we use planets from 1-10 M_{\oplus} and detail the heteroscedastic relationship of stability time for this large range of planet masses. We conclude with discussion in Section 7.

2 DYNAMICAL SPACING AND STABILITY: RELEVANT PARAMETERS

For small eccentricities and inclinations, the mutual Hill radius of two bodies is defined as

$$R_{H_{1,2}} = \left(\frac{m_1 + m_2}{3M} \right)^{1/3} \frac{a_1 + a_2}{2}, \quad (1)$$

where m_1 and m_2 are the planetary masses, a_1 and a_2 are their semi-major axes, and M is the mass of the central body. The separation of two planet's semi-major axes can be measured in units of mutual Hill radii by a spacing parameter, Δ , given as

$$a_2 - a_1 = \Delta R_{H_{1,2}}. \quad (2)$$

The spacing is denoted as ‘K’ in Marzari & Weidenschilling (2002) and ‘ β ’ in Smith & Lissauer (2009).

For a system of n planets, Eq. 1 and Eq. 2 can combine to give

$$a_{i+1} = a_i \frac{2 + \Delta K}{2 - \Delta K}, \quad (3)$$

where

$$K = \left(\frac{m_i + m_{i+1}}{3M} \right)^{1/3} \quad (4)$$

for a pair of planets of masses m_i (inner) and m_{i+1} (outer) around a central body of mass M . Once the innermost planet's orbit (starting from a_1) and a spacing parameter is chosen, the masses of adjacent planets then dictate the semi-major axis of the next planet.

A two-planet system is stable if $a_2/a_1 > 1 + 2\sqrt{3}K$ to the lowest order in planet masses (Gladman 1993). With Eq. 3, the critical spacing parameter for two planet stability is given by

$$\Delta_c = \frac{2\sqrt{3}}{1 + \sqrt{3}K}. \quad (5)$$

However, for systems of more than two planets the energy and angular momentum of a given planet pair are not conserved because of perturbations from the additional planets. This results in orbit crossings even in systems with initially large separations.

Chambers et al. (1996) find an exponential relationship between the dynamical spacing in multiple planet systems and the time from initial conditions to the first close encounter (defined as a separation of less than one Hill Radius). We refer to this time as the “close encounter time” or “stability time” and denote it as t_c . The relationship is given by

$$\log(t_c) = b(\Delta) + c. \quad (6)$$

The values of the constants b and c depend on planet mass and multiplicity (Chambers et al. 1996) and initial eccentricity (Yoshinaga et al. 1999). To compare with previous work, we use the mutual Hill radius to measure separations, Δ , though the relationship becomes independent of planet mass when separations are measured in units of $(m_p/m_o)^{1/4}$

Close encounters always happen on the same timescale as orbital crossings. However, we note that Rice et al. (2018) and Bartram et al. (2021) show that the architecture of the system may not change through a collision or ejection of a planet on this same timescale in non-coplanar systems. The stability or survival time relationship has also been detailed in Quarles & Lissauer (2018) in the specific case of binary star systems, in eccentric systems in Gratia & Lissauer (2019), and in other works such as Funk et al. (2010); Zhou et al. (2007); Quillen (2011); Yalinewich & Petrovich (2019); Petit et al. (2020); Hussain & Tamayo (2020); Lissauer & Gavino (2021).

For multiple planet systems with equal-mass planets, the equal spacing given by Eq. 3 keeps the ratio of semi-major axis constant. From Kepler's Third Law, the period ratio is also constant,

$$P_r = \frac{P_{i+1}}{P_i} = \left(\frac{2 + \Delta K}{2 - \Delta K} \right)^{3/2}. \quad (7)$$

In equal-mass, equal-spacing systems the period ratio will be equal for all pairs of adjacent planets. Additionally, the period ratios of next-adjacent planets (i.e. P_3/P_1 and P_4/P_2) will be equal.

If the period ratio of two planets is equal to a ratio of small integers the planets are said to be near MMR. When planets in equal-mass, equal-spacing systems are near first and second order MMR the stability time of the system can be an order of magnitude longer or shorter than expected from the exponential Eq. 6 (Obertas et al. 2017). Using variable masses changes K in Eq. 7, breaking the chain of equal period ratio between the planets.

3 SIMULATIONS

To run our N-body integrations we use the orbital dynamics package MERCURY6.2 (Chambers 1999). We use the Bulirsch-Stoer method and the accuracy parameter is set to 10^{-12} . The initial timestep is set to less than $1/20^{\text{th}}$ of the initial period of the innermost planet. The planets are placed around a central body of $1.0 M_{\odot}$.

The initial conditions of the planets are detailed in Table 1. Our artificial planetary systems in this study will consist of four planets. We use a Rayleigh distribution to draw eccentricities and inclinations (Fang & Margot 2013). However, we use a small Rayleigh scale parameter of 10^{-6} which keeps the system initially near-circular and near-coplanar to be comparable with Rice et al. (2018). The three remaining orbital parameters—the longitude of the ascending node, argument of periapsis, and mean anomaly—are chosen uniformly from $0 - 2\pi$. We do not impose a minimum angular separation on our planets, this choice was reported to not alter the orbital crossing time for systems with $\Delta > \Delta_c$ in Obertas et al. (2017).

Stability time in this study is interchangeable with close-encounter time, t_c . The time is measured from the integration start to the first close encounter between two planets of less than one Hill radius. We scale the times by the period of the innermost planet, t_c/T_i where T_i is 11.55 days. Ejections and collisions with the central body are not observed in any runs.

The following three sections use different planet masses and different mass variations which are described in their respective sections. For each investigation, a “suite” of at least 1,000 systems is simulated uniformly across a given range of separations (Δ) with a given prescription for the masses of planets in each system. The innermost planet is placed at 0.1 AU. The separation and mass of adjacent planets then determines the semi-major axis of the subsequent planets with Eq. 3.

Table 1. Initial conditions for the system and each of the four planets across simulations

Parameter	Details
Central Mass (M_{\odot})	$1.0 M_{\odot}$
Planet Multiplicity	4
Planet Mass	Reported in Section
Semi-Major Axis (AU)	$a_1 = 0.1$ & Eq.(3)
Eccentricity	Rayleigh, $\sigma = 10^{-6}$
Inclination ($^{\circ}$)	Rayleigh, $\sigma = 10^{-6}$
Arg. of Pericenter ($^{\circ}$)	Random uniform 0-360
Long. of Ascend. Node ($^{\circ}$)	Random uniform 0-360
Mean Anomaly ($^{\circ}$)	Random uniform 0-360

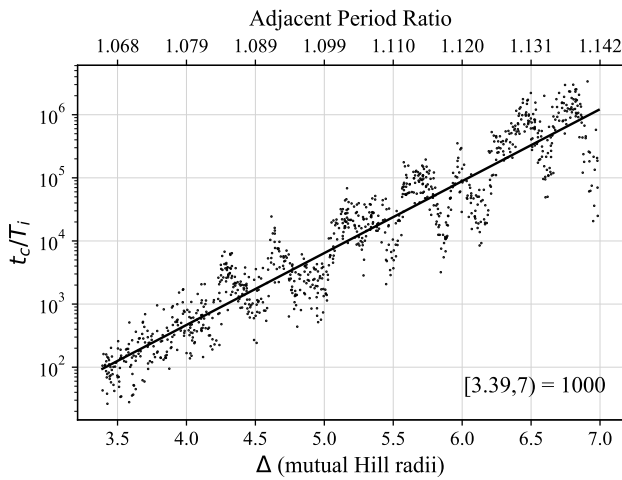


Figure 1. The time to the first close encounter of less than one Hill radius between two planets in terms of the innermost planet’s orbital period against spacing measured in mutual Hill radii. Close encounter (stability) time measured for 1,000 systems of four, equal Earth-mass planets. Least-squares regression shown between $\Delta_c \leq \Delta \leq 7$ (Eq. 5). Top axis shows the period ratio between adjacent planets in the systems. Note that this axis is not linear and is determined by Eq. 7.

4 STABILITY TIME WITH SPACING RELATIONSHIP

As an initial test, we show the stability time with spacing relationship for our systems in Fig. 1. We run 1,000 simulations of systems with four equal- $1M_{\oplus}$ planets around a Sun-like star with the innermost planet at 0.1 AU. The separations are chosen uniformly between Δ_c and $7 R_H$ with $\Delta_c \approx 3.39$ (Eq. 5).

All simulations had a close encounter within 10^7 orbits of the innermost planet. The exponential relationship is $\log(t_c/T_i) = 1.14\Delta - 1.89$. When the maximum Δ cutoff is varied between 6.0 and 7.0, the slope ranges from 1.09 to 1.17 and the intercept from -2.04 to 1.69. These values are similar to the relationship for five planets in Obertas et al. (2017).

The top axis in Fig. 1 shows the period ratio of adjacent planets in the systems. The modulations in the relationship from MMRs are apparent in our data. For example, the dip around the 1.110 period ratio and 5.5 mutual Hill radii corresponds with a first order MMR with period ratio of 10:9 between adjacent planets in the system. Not shown in Fig. 1 is the period ratio between next-nearest planets which were also shown to correlate with dips in Obertas et al.

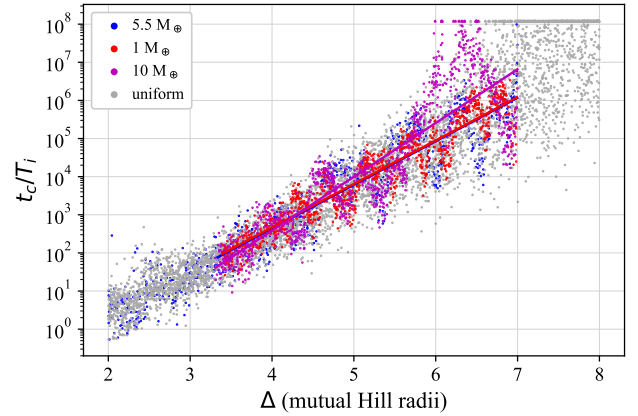


Figure 2. Stability time of three 1,000 system suites of equal-mass planets: $1 M_{\oplus}$ (red), $5.5 M_{\oplus}$ (blue), and $10 M_{\oplus}$ (purple) with spacing. Grey dots in back are discussed in Sect. 6 and Fig. 6. Systems which reached the maximum integration time are plotted at 10^8 orbits. Different masses have different resonance features. Simple least-squares regressions shown for each suite between Δ_c and $\Delta = 7$.

(2017). There is often a degeneracy in deciding which period ratio is responsible for a dip.

In Fig. 2, we also show suites with equal- $5.5M_{\oplus}$ and equal- $10M_{\oplus}$ planets. The period ratio of adjacent planets at a given separation is different in each of these suites and results in different modulations of the stability time relationship. In this range of masses and spacing, the relationship shows little variation with mass. However, the $10 M_{\oplus}$ suite exhibits a larger slope because of a region of systems with longer stability times, a few of which did not have a crossing within the integration time and are plotted at 10^8 orbits. The large increase in stability time for the $10 M_{\oplus}$ systems is between the 5:4 ($\Delta \approx 5.5$) and 4:3 MMR ($\Delta \approx 7.0$) with a small dip in the middle corresponding to systems with periods near a second order 9:7 resonance ($\Delta \approx 6.2$).

5 VARIABLE MASS WITH EQUAL SPACING

We now turn to detailing the stability time relationship without the additional structure from MMR. To do so we use a varied planetary mass while keeping equal dynamical spacing in terms of mutual Hill radii as first explored in Chambers et al. (1996). Having non-equal mass means that the planets no longer create chains of equal period ratios (See Eq. 7). This prescription is complimentary to, but not equal to, systems with non-equal separations and equal mass which is explored in Wu et al. (2019).

The mass of each planet in four-planet systems is chosen from a normal distribution, $\mathcal{N}(\mu, \sigma^2)$. The mean value is kept at one Earth-mass while we vary the standard deviation across the suites. Systems are simulated randomly from $\Delta_{c,1M_{\oplus}} \leq \Delta \leq 7$. The innermost planet is at 0.1 AU. The semi-major axes of subsequent planets are given by the chosen Δ , the mass of the planet, and the mass of it’s interior neighbor (Eq. 3). All simulations had a close encounter within the max integration time of 10^8 orbits of the innermost planet. The results are shown in Fig. 3.

As the standard deviation of the mass distribution increases from 0.01 to $0.3 M_{\oplus}$, the structure in the stability time relationship is erased. In Fig. 4, we show the amount the average residual in 0.1Δ

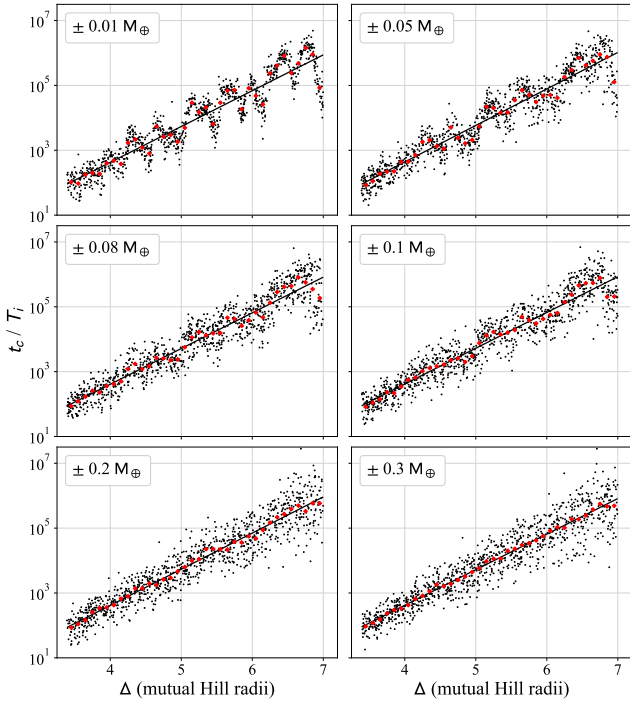


Figure 3. Stability time for suites of simulations with non-equal-mass planets. The mass of each planet in the system is chosen from a normal distribution with $\mu = 1 M_{\oplus}$ and σ shown in the legend. Systems are spaced by Δ and by the mutual Hill radius of each set of adjacent planets in the system. The mean value of systems in bins 0.1Δ wide are shown in red. Compare to the equal-mass systems of Fig 1.

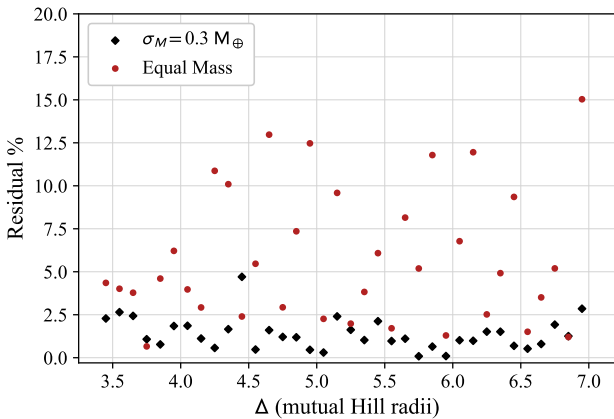


Figure 4. The deviation of binned means from the linear regression for systems with equal masses, *circles*, and with normal deviations of $0.3 M_{\oplus}$ in planet mass, *diamonds*. Bins are 0.1Δ wide as in Fig. 3. The residual percentage is the ratio of the absolute difference between the mean and predicted value from the linear regression to the predicted value.

wide bins varies from the regression as a percent of the expected regression value. The residuals for the $\sigma = 0.3 M_{\oplus}$ systems (1.15 per cent) are on average 4 times smaller than that of the equal-mass systems (4.76 per cent). A Durbin-Watson test (Durbin & Watson 1950) returns a test statistic that ranges from 0-4 with a value of 2 indicating no autocorrelation. The test statistic for the uniform

Table 2. Two measurements of the removal of MMR modulations—the median absolute residual of bins and the Durbin-Watson test of autocorrelation—for the constant and variable mass suites.

σ_m	Median $ (\bar{y}_{\text{bin}} - \hat{y}) $ (%)	D-W Statistic
0.0	4.76	0.74
0.01	5.80	0.70
0.05	3.78	1.26
0.08	3.30	1.66
0.1	3.53	1.61
0.2	2.03	2.00
0.3	1.15	2.12

mass suite is 0.74 indicating positive autocorrelation while the test statistic for the $\sigma = 0.3 M_{\oplus}$ suite is 2.1. We summarize these findings for all suites in Table 2.

From our simulations, a standard deviation which is 30 percent of the average mass effectively removes the MMR modulations. Note with this deviation 0.04 per cent of systems will be below zero mass and are removed from the initial conditions. We do not show a full investigation here, but a 30 per cent deviation also erases the modulations of stability times in equally-spaced systems with mean masses of 0.1 and $10 M_{\oplus}$.

Rice et al. (2018) show that the stability times of systems with the same equal-spacing and equal-mass are distributed log-normally with a standard deviation of approximately 0.22 dex which Hussain & Tamayo (2020) shows matches the simulations of Obertas et al. (2017). The varied mass suite with deviation of $0.3 M_{\oplus}$ has a standard deviation of stability time of 0.42 dex. This is in agreement with Hussain & Tamayo (2020) findings of 0.43 dex when running “shadow integrations” of a single system with small perturbations. The variable mass disrupts the chain of period ratios which almost doubles the deviation in stability times.

5.1 Change in Period Ratio

In reality, a planetary system will have non-uniform masses, dynamical spacings, and period ratios. In Eq. 7, we see all these quantities are related. Thus a variation in the planets’ masses correspond to a variation in spacing or period ratio. If we propagate the previously found standard deviation of $0.3 M_{\oplus}$, we can find the deviation in period ratios which disrupts the chain of MMRs resulting in wide distributions of stability time. This deviation will also depend on the separation, Δ .

We use the variance formula to find the deviation,

$$\sigma_{P_r} = \sqrt{\left(\frac{\delta P_r}{\delta K}\right)^2 \sigma_K^2}, \quad (8)$$

where P_r is given in Eq. 7. The variance of K , σ_K^2 , is given by the derivative of Eq. 4 with respect to $m_1 + m_2$ multiplied by $\sigma_{m_1+m_2}$. Lastly, $\sigma_{m_1+m_2}$ is given by adding the variance of each planet’s deviation in mass, here $\sqrt{2(0.3M_{\oplus})^2}$. We also include a term under the square root in Eq. 8 for the deviation in Δ from our binning process, but this term is negligible for $K \ll \Delta$.

For a system with masses drawn from $\mathcal{N}(1M_{\oplus}, (0.3M_{\oplus})^2)$, the expected deviations in the period ratios from Eq. 8 are plotted on Fig. 5. The deviation is fairly-linear with separation in this region. We measure the three period ratios in each 4-planet system in our suite with equal-spacing and a σ_m of $0.3 M_{\oplus}$. The standard deviation of period ratios is then measured in bins of width 0.1Δ . There are

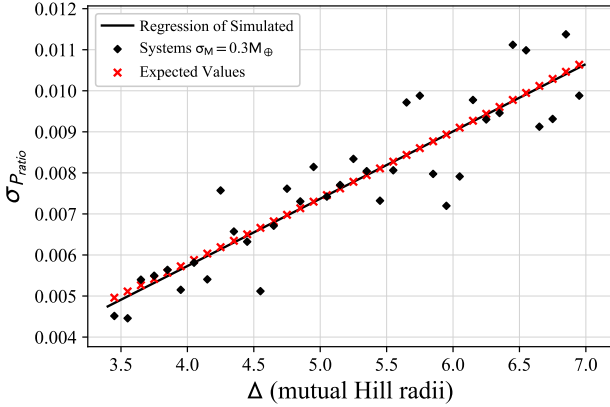


Figure 5. The period ratio between every pair of adjacent planets in the 1,000 $\sigma_m = 0.3M_\oplus$ systems are measured. Shown here is the standard deviation of period ratio in 0.1 wide bins of Δ . Black line shows the regression of the simulated standard deviations while red crosses show the expected deviation from error propagation using the variance formula. It is expected that adding a normal deviance of this size to the period ratios in systems will result in no MMR structures in the stability relationship.

on average 28 systems and 84 period ratios in a bin. As shown, a linear regression of the deviations are consistent with the expected values.

To illustrate this result's affect on stability time, consider the dip at $\Delta = 5.5$ in Fig. 1 which we claim is caused by being near a 10:9 MMR, $P_r \approx 1.11$. The average system with this separation would likely have a stability time which is 10,000 orbits less than expected from the trend line (13.4 versus 23.9 thousand orbits). A normal deviation in the period ratio of the planets of ~ 0.008 is enough for the average system to remain stable for longer, returning to the trend line. This deviation in period ratio is mass dependent and would double to around 0.02 for a chain of $10 M_\oplus$ planets.

6 SYSTEMS WITH MASSES FROM 1-10 M_\oplus

As seen in the previous section, adding a normal variation to the individual planetary mass in systems with equal mutual Hill radii spacing smooths over the modulations from two-body resonances. We take our simulations further by varying mass by up to a factor of ten. Each planet's mass is chosen from a uniform distribution between 1 and $10 M_\oplus$. The stability time for 5,000 of these heterogeneous-mass systems are shown in Fig. 6 with a maximum integration time of 10^9 orbits. 96.3 per cent of systems remain stable throughout the entire integration. The exponential relationship between the spacing and the stability time is maintained for these systems, and no MMR structures are visually apparent. In addition, we simulate 500 systems that extend our spacing to $\Delta = 10$ and integration time to 10^{10} orbits.

In Fig. 7, systems are colored by their average mass. Linear regressions for systems with an average mass above $7 M_\oplus$ and below $4 M_\oplus$ and with $\Delta_{c,5.5M_\oplus} < \Delta < 7$ return similar slopes and intercepts. The per cent difference in the slope of these two regressions is 5 per cent; within the 6 per cent standard error of the slope for the low mass systems.

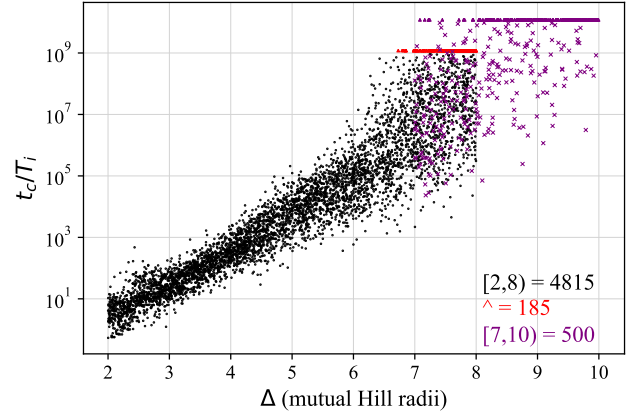


Figure 6. Stability time in terms of the innermost planet's period against the spacing of the system in mutual hill radii of adjacent planets. Each planet's mass in the four planet systems is chosen uniformly from $1 M_\oplus$ to $10 M_\oplus$. 5,000 systems (*black dots*) are simulated with $\Delta = [2, 8)$ and maximum integration time of 10^9 orbits. An additional 500 systems (*purple x's*) are simulated with $\Delta = [7, 10)$ and maximum integration time of 10^{10} orbits. Systems shown as triangles did not have a close-encounter of less than 1 Hill Radius within the maximum integration time and are plotted at the maximum.

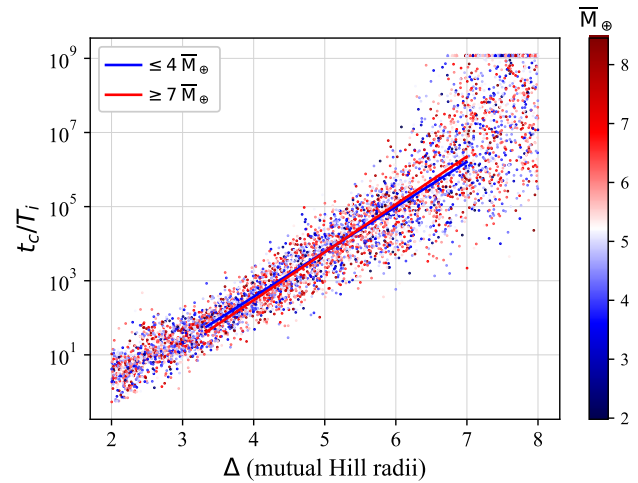


Figure 7. The systems from Fig. 6 are colored by the average mass of their 4 planets, and linear regressions are shown for systems with average mass $\ge 7 M_\oplus$ and $\le 4 M_\oplus$ between $\Delta_c < \Delta < 7$.

6.1 The Heteroscedasticity of Stability Time

As the period ratios increase, the difference in a near-resonant system's stability time from the expected exponential relationship seems to grow. Consider in Fig. 1 the modulation from the 10:9 (1.110) versus that of the 8:7 (1.142) period ratio. The modulations are smoothed over when using varying masses, Fig. 3, but nonetheless the variance of stability time at a given separation increases with said separation.

With a range of masses from 1-10 M_\oplus , this increase is apparent. The dispersion of stability time with separation is shown in Fig. 8. Systems with the same separation but different masses have stability times distributed with a standard deviation from 0.32 up to 1.20 dex.

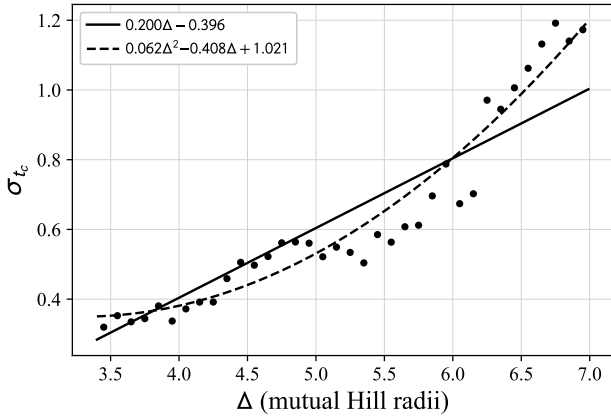


Figure 8. The standard deviations of stability time in bins 0.1Δ wide are measured for the 3,034 systems with $\Delta_c < \Delta < 7$. Each bin has over 70 systems. The measured values from the simulations are compared to the linear and quadratic standard deviation models. Although it is not clear visually which model is better, the data is clearly heteroscedastic.

Thus the stability times of systems with $\Delta = 7$ vary from $10^3 - 10^9$ orbits of the innermost planet.

Data with non-constant dispersion is referred to as “heteroscedastic”. The classical least-squares regression assumes the residuals are normally distributed and have a constant standard deviation. We build a Bayesian Linear Regression that minimizes the coefficient of determination, r^2 , by sampling values for the slope, intercept, and standard deviation using PyMC3 [Salvatier et al. \(2016\)](#). The slope and intercept are sampled from wide normal distributions centered at 0 with variance of 10^8 while the standard deviation is sampled from wide, positive half normal distributions. To do so we use a Markov Chain Monte Carlo (MCMC) with a number of chains equal to the number of parameters and at least a total of 10,000 sample draws across all chains.

We analyze the 3,034 systems between $\Delta_{c,5.5M_\oplus} \approx 3.34$ and $\Delta = 7$. In this region less than 0.3 per cent of systems did not have a close encounter within our integration time and are given a stability time of 10^9 orbits for analysis. A Bayesian regression with constant deviation gives best fit values of $\log(t_c/T_i) = 1.267^{+0.023}_{-0.023}\Delta - 2.551^{+0.120}_{-0.127}$ and $\sigma = 0.692^{+0.017}_{-0.019}$. The \pm values show the 95 per cent Highest Posterior Density (HPD) regions.

To detail the heteroscedasticity of the data, we build two models—one with linearly increasing and another with quadratic increasing standard deviation of stability time with separation. The response variable in each model is modeled as $y \sim \mathcal{N}(b\Delta + c, b_\sigma\Delta + c_\sigma)$ and $y \sim \mathcal{N}(b\Delta + c, a_\sigma\Delta^2 + b_\sigma\Delta + c_\sigma)$, respectively. The MCMC with the linearly increasing deviation produces a model of stability time where $\log(t_c/T_i) = 1.233^{+0.020}_{-0.019}\Delta - 2.382^{+0.091}_{-0.088}$. These parameters are slightly better constrained than the constant model. The deviation is given by $\sigma = 0.200^{+0.012}_{-0.012}\Delta - 0.396^{+0.054}_{-0.056}$. The parameters for the constant, linear, and quadratic models are given in Table 3.

We use the mean value of the posteriors for simplicity when plotting. Fig. 8 shows the equations for the standard deviation for our two models. We compare this to the measured deviation in our data by binning the systems in 0.1 wide bins in Δ and measuring the bin’s deviation in stability time. Fig. 9 shows the models extended past our analysis range.

To compare the goodness-of-fit of our models, we use the

Table 3. Three models of the data with values for the best-fit line and fits for how the standard deviation in stability time varies with orbital spacing with the average of the HPD region and the Widely-Applicable Information Criteria.

Model	a_σ	b b_σ	c c_σ	WAIC	SE
Constant		1.267(23)	-2.551(124)	6378	114
Linear		1.233(20)	-2.382(90)	5491	94
Quadratic	0.062(14)	-0.408(142)	1.021(342)	5415	91

Watanabe-Akaike information criterion, also known as the widely applicable information criterion (WAIC) ([Watanabe 2010](#)). In general, the lower the WAIC is the better the model fits the data. In Table 3, we report the WAIC and the standard error in the criterion for our three Bayesian linear regressions with different models for the standard deviation. There is a large drop in WAIC when using a non-constant deviation model. The quadratic model has the lowest WAIC, but it is well within the standard error of the WAIC for the linear model. Within our analysis range, it remains unclear of how to best model the heteroscedasticity of the stability time.

6.2 Stability at Large Separations

Our analysis thus far has been bound by the critical separation and $\Delta = 7$. A large portion of systems with separations of $\Delta > 7$ have stability times which exceed our maximum integration time. Previous studies have suggested that the exponential relationship breaks and there is a rapid increase in stability time at large separations where “large” is dependent on system properties such as mass and multiplicity ([Smith & Lissauer 2009](#); [Obertas et al. 2017](#); [Petit et al. 2020](#)). We extrapolate the relationships from the previous section and confirm that systems are more stable than predicted past $\Delta = 7$.

In Fig. 10, the stability times for the 5000 systems with uniform mass are divided from $\Delta = 3$ to 8 into bins with width of $1-\Delta$. The 500 systems with an extended integration time of 10^{10} orbits are included from $\Delta = 8$ to 10. Predicted distributions of stability times from the quadratic deviation model are similar to the histograms up to $\Delta = 7$. The three histograms for $\Delta = 7 - 10$ are shifted to the left with a dearth of systems with short stability times and more with longer stability times.

185 systems have stability times greater than the integration time of 10^9 orbits for our 5,000 systems with $2 < \Delta < 8$. Systems are much more stable than predicted—the linearly increasing standard deviation model predicts 30 systems while the quadratic deviation model predicts 67 systems with stability times over 10^9 orbits. At least twice as many systems are stable for over 10^{10} orbits for our 500 systems simulated uniformly from $7 < \Delta < 10$ than expected. 48.2 per cent have stability times over the integration time while the linear and quadratic models predict 14 per cent and 20 per cent, respectively.

There is also a lack of systems with short stability times of less than 10^6 orbits. For the 500 systems, 6 per cent have short stability times while the linear model predicts around 10 per cent and the quadratic model predicts 18 per cent. No systems between $9 < \Delta < 10$ have short stability time. Although the linear model predicts only 2 systems in this region should be short, the quadratic

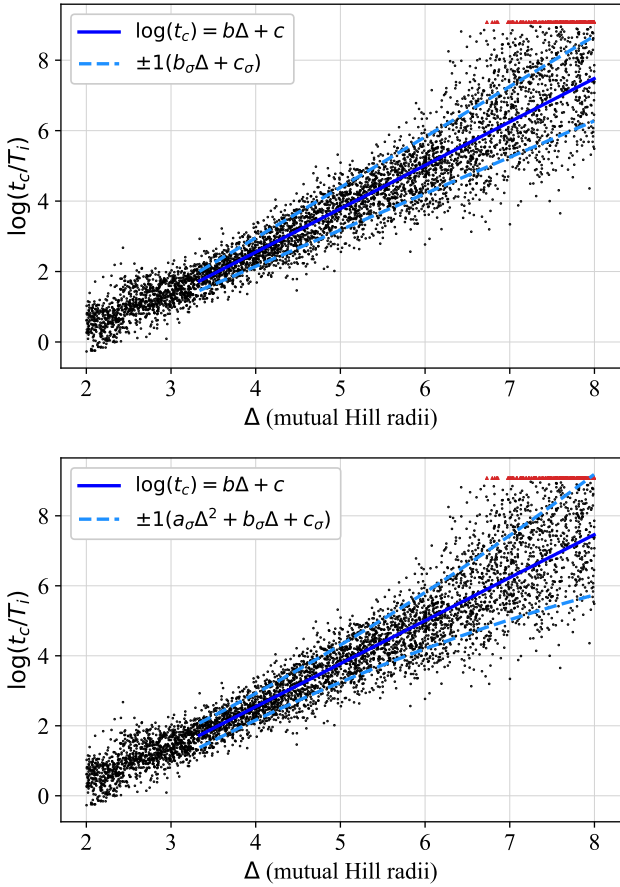


Figure 9. Stability time shown for 5,000 systems simulated with $\Delta = [2, 8)$ and model linear regression. *Top* plots the model with linearly increasing standard deviation and *Bottom* plots the quadratic increasing standard deviation. We only plot the mean values from the posterior distributions for simplicity. Analysis is done between $\Delta_c < \Delta < 7$, but lines are extrapolated here to $\Delta = 8$.

model predicts 20 systems. These results confirm an increase in stability time from the predicted linear fits at large separations.

Most studies of stability time limit their computation time by $10^8 - 10^9$ orbits of the innermost planet. Trappist-1 which has spacings that range from $\Delta \approx 6.8 - 13.4$ has evolved for over 10^{12} orbits of Trappist-1b (Grimm et al. 2018; Burgasser & Mamajek 2017). Understanding the stability time at large spacings and how being near strong MMR’s causes variability should be of interest to future studies.

7 CONCLUSION

The time until an orbital crossing in a multiple planet system can be predicted by the dynamical spacing of the system measured in mutual Hill radii. Studies that use systems with equally-spaced and equal-mass planets find that the stability time varies from the prediction when systems are near MMR causing separation-dependent modulations in the stability time at predictable period ratios. We disrupt the chains of MMR by using non-equal masses while keeping the system equally spaced in terms of mutual Hill radii.

Because of the variations in the stability time relationship from MMR, the least-squares regressions used in previous studies (Cham-

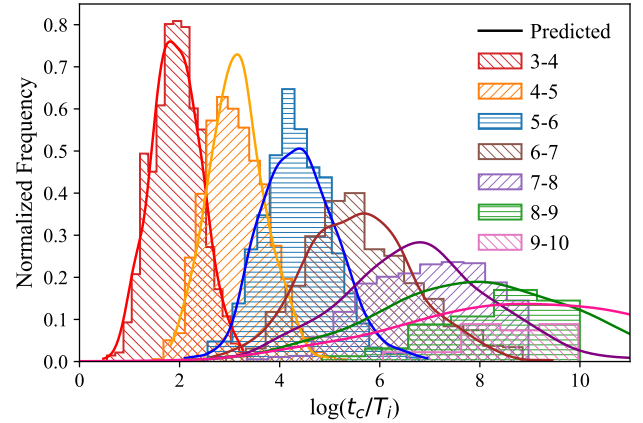


Figure 10. Normalized histograms of stability times for the systems in Fig. 6 divided into one mutual Hill radii bins which are denoted in the legend (i.e. $\Delta = 3$ to 4). Histograms normalized to the percent with stability time within the maximum integration time. Five million systems are simulated using the quadratic deviation model and separated into the same bins. The distributions of these “predicted” systems are smoothed with a Gaussian kernel density estimator. Scott’s Rule used for all distributions Scott (2015).

bers et al. 1996; Obertas et al. 2017; Wu et al. 2019; Gratia & Lissauer 2019) do not account for heteroscedasticity and depend on the range chosen for analysis. In Fig. 2, our least-squares regression for equal- $10 M_{\oplus}$ systems is strongly influenced by the large increase in stability time near $\Delta \approx 6$. This bump is surrounded by the 5:4 and the 4:3 first order MMR between adjacent planets which occur at separations of approximately $\Delta = 5.5$ and $\Delta = 7$. Choosing mass from a normal distribution centered at $1 M_{\oplus}$ with $\sigma = 0.3 M_{\oplus}$ while keeping equal spacing smooths the stability time with spacing relationship over MMR modulations (Fig. 3 and 4).

The non-equal masses change the period ratio between planets in each system, shown in Fig. 5. The deviation in period ratio is non-linear, but it is approximately a linear effect with Δ in our analysis region. By varying the mass of the planets the ratios vary twice as much at $\Delta = 7$ than at $\Delta = 3.5$. Since, resonances closer to 2:1 cause a larger decrease in stability time, as seen in Obertas et al. (2017), and have larger resonance widths, this is an effective method for setting up systems where the planet’s aren’t in chains of equal period ratios.

We further our study by choosing each planet’s mass from a uniform distribution between one and ten Earth-masses. As with normally distributed masses, this prescription smooths out resonance modulations, but the exponential relationship between spacing and stability time remains, Fig. 6. We find that the relationship in log-time is now best captured by a linear relationship with a linearly or quadratic increasing standard deviation, shown in Fig. 9. However, this relationship fails to capture the increase in stability times for systems with separations over seven mutual Hill radii. With a linear model, the standard deviation of stability time becomes one 1.0 dex at $\Delta = 6.98$. At this spacing the time to a close encounter can vary from 10^3 to 10^9 orbits of the innermost planet.

Proposed mechanisms which drive the instability resulting in the stability time with spacing relationship include those by Zhou et al. (2007) and Yalinewich & Petrovich (2019). Of promise is the theory proposed by Quillen (2011) and Petit et al. (2020) that overlapping three-body resonances drives the chaos. Petit et al. (2020) show that this mechanism predicts an exponential relationship at

small separations and a jump in stability time at larger separations. The shorter stability time caused by two body-resonance is then seen as a dip away from the predicted stability from three-body resonances. Two aspects explored in this work, the amplitude of the dips and stability times at large separations, are possible tests for this analytical prediction.

These variable stability times impact planet formation. During oligarchic growth, large planet embryos are generally assumed to have spacings based upon their feeding zones at some multiple of their Hill radii. Collisional fragmentation clears out the disc and dynamic instabilities become the dominate form of embryo-embryo interaction [Goldreich et al. \(2004\)](#). The results here suggest that in initially similar systems the time until dynamic instability occurs could be multiple orders of magnitude longer or shorter than predicted from relationships of stability time and spacing.

ACKNOWLEDGEMENTS

DRR and JHS appreciate A. Yalinewich, C. Petrovich, A. Obertas, D. Tamayo, and A. Petite for stimulating discussions. We acknowledge support from the College of Sciences at the University of Nevada, Las Vegas, the Nevada Center for Astrophysics, and NASA grants NNX16AK32G and NNX16AK08G. All simulations were supported by the Cherry Creek Cluster at UNLV. We acknowledge that the study resulting in this publication was assisted by a graduate fellowship from The Nevada Space Grant Consortium.

DATA AVAILABILITY

Full data, summary data, and plotting tools underlying this article will be shared on request to the corresponding authors.

REFERENCES

- Bartram P., Wittig A., Lissauer J. J., Gavino S., Urrutxua H., 2021, *MNRAS*, **506**, 6181
- Burgasser A. J., Mamajek E. E., 2017, *ApJ*, **845**, 110
- Chambers J. E., 1999, *MNRAS*, **304**, 793
- Chambers J. E., Wetherill G. W., Boss A. P., 1996, *Icarus*, **119**, 261
- Deck K. M., Payne M., Holman M. J., 2013, *ApJ*, **774**, 129
- Durbin J., Watson G. S., 1950, *Biometrika*, **37**, 409
- Fabrycky D. C., et al., 2014, *ApJ*, **790**, 146
- Fang J., Margot J.-L., 2013, *ApJ*, **767**, 115
- Funk B., Wuchterl G., Schwarz R., Pilat-Lohinger E., Eggl S., 2010, *A&A*, **516**, A82
- Gladman B., 1993, *Icarus*, **106**, 247
- Goldreich P., Lithwick Y., Sari R., 2004, *ApJ*, **614**, 497
- Gratia P., Lissauer J. J., 2019, arXiv e-prints, p. [arXiv:1908.01117](#)
- Grimm S. L., et al., 2018, *A&A*, **613**, A68
- Hussain N., Tamayo D., 2020, *MNRAS*, **491**, 5258
- Lissauer J. J., Gavino S., 2021, *Icarus*, **364**, 114470
- Luger R., et al., 2017, *Nature Astronomy*, **1**, 0129
- MacDonald M. G., et al., 2016, *AJ*, **152**, 105
- MacDonald M. G., Feil L., Quinn T., Rice D., 2022, *AJ*, **163**, 162
- Marzari F., Weidenschilling S. J., 2002, *Icarus*, **156**, 570
- Mills S. M., Fabrycky D. C., Migaszewski C., Ford E. B., Petigura E., Isaacson H., 2016, *Nature*, **533**, 509
- Obertas A., Van Laerhoven C., Tamayo D., 2017, *Icarus*, **293**, 52
- Petit A. C., Pichierrri G., Davies M. B., Johansen A., 2020, *A&A*, **641**, A176
- Pu B., Wu Y., 2015, *ApJ*, **807**, 44
- Quarles B., Lissauer J. J., 2018, *AJ*, **155**, 130
- Quillen A. C., 2011, *MNRAS*, **418**, 1043

- Rice D. R., Rasio F. A., Steffen J. H., 2018, *MNRAS*, **481**, 2205
- Salvatier J., Wiecki T. V., Fonnesbeck C., 2016, *PeerJ Computer Science*, **2**, e55
- Scott D. W., 2015, *Multivariate Density Estimation: Theory, Practice, and Visualization*. John Wiley & Sons, Inc.
- Smith A. W., Lissauer J. J., 2009, *Icarus*, **201**, 381
- Steffen J. H., Hwang J. A., 2015, *MNRAS*, **448**, 1956
- Volk K., Gladman B., 2015, *ApJ*, **806**, L26
- Watanabe S., 2010, *J. Mach. Learn. Res.*, **11**, 3571
- Wu D.-H., Zhang R. C., Zhou J.-L., Steffen J. H., 2019, *MNRAS*, **484**, 1538
- Yalinewich A., Petrovich C., 2019, arXiv e-prints, p. [arXiv:1907.06660](#)
- Yoshinaga K., Kokubo E., Makino J., 1999, *Icarus*, **139**, 328
- Zhou J.-L., Lin D. N. C., Sun Y.-S., 2007, *ApJ*, **666**, 423

This paper has been typeset from a $\text{\TeX}/\text{\LaTeX}$ file prepared by the author.